sustainability

MDPI

Article

Study on the Characteristics of Granite in Different Stress Stages through a Cyclic Loading Experiment

Handong Liu [1,2], Jialiang Wang [1,2,*], Huaichang Yu [1,2] and Yiying Zhang [3]

[1] Research Institute of Geotechnical Engineering and Hydraulic Structure, North China University of Water Resources and Electric Power, Zhengzhou 450046, China; liuhandong@ncwu.edu.cn (H.L.); yuhuaichang@ncwu.edu.cn (H.Y.)
[2] College of Geosciences and Engineering, North China University of Water Resources and Electric Power, Zhengzhou 450046, China
[3] Yellow River Engineering Consulting Co., Ltd., Zhengzhou 450003, China; zhangyiying@yrec.cn
* Correspondence: jialiang_j.wang@foxmail.com

Abstract: The deformation and failure process of rocks is a gradual process. The purpose of this study was to examine the characteristics of rocks in different stages through a cyclic loading experiment. The experiment was carried out based on the MTS815 rock mechanics test system combined with acoustic emission monitoring equipment to study the typical characteristics of two kinds of granite in the stages of crack closure, linear elastic deformation, crack initiation and stable crack growth, along with crack damage and unstable crack growth. The results showed that there were significant differences in the characteristics of the strain response, energy evolution, and acoustic emission of the two granites in the different stages. Although the microstructure and mineral elements of the two granites are different, the characteristics of the two granites in the same stage were similar, indicating that the stage characteristics of brittle rocks in the failure process may be widespread and have significant similarities.

Keywords: granite; cyclic loading; MTS; strain characteristics; acoustic emission

Citation: Liu, H.; Wang, J.; Yu, H.; Zhang, Y. Study on the Characteristics of Granite in Different Stress Stages through a Cyclic Loading Experiment. *Sustainability* **2023**, *15*, 12832. https://doi.org/10.3390/su151712832

Academic Editors: Qiong Wu, Rui Yong, Tao Wen and Kun Fang

Received: 25 July 2023
Revised: 23 August 2023
Accepted: 23 August 2023
Published: 24 August 2023

1. Introduction

The deformation and failure process of rocks is a gradual process. The initiation, extension, and coalescence of new and old microcracks in rocks make the macro-deformation characteristics of rocks show significant stage characteristics. Many scholars [1,2] have demonstrated that the pre-peak stages of brittle rocks can be divided into four stages according to the crack evolution [3–5]: include crack closure, linear elastic deformation, crack initiation and stable crack growth, and crack damage and unstable crack growth. In the crack closure stage at the initial stage of loading, the discontinuity inside the rock gradually closes, and the deformation modulus of the rock gradually increases macroscopically. After most of the discontinuities in the rock are closed, the rock enters the linear elastic deformation stage. The axial strain and circumferential strain of the rock are approximately linear with the axial stress. The axial stresses corresponding to the start point and end point of this stage are called crack closure stress and crack initiation stress, respectively. After entering the stage of crack initiation and stable crack growth, the microcracks in the rock begin to sprout and develop, the axial and circumferential strain responses deviate from linearity, and a turning point in the rock volume from compression to expansion occurs [1,6,7]. The axial stress corresponding to the end point of this region is crack damage stress. In the stage of crack damage and unstable crack growth, the circumferential strain increases rapidly, the volumetric strain of the specimen changes from negative to positive, and the volume expands. Different from the previous stage, the crack propagation in this stage cannot be controlled, which means that, even if the applied load remains unchanged, the crack will continue to expand until the rock fails. The difference in the rock mechanical

response in different stages is of great significance for practical engineering problems. Andersson et al. [8] and Martin and Christiansson [9] proposed that the in situ spalling strength can be estimated using the rock crack initiation stress measured in a laboratory uniaxial compression test. In relevant studies [10–13], initiation stress and damage stress are two of the mechanical parameters of rocks in rock constitutive equations.

The identification of rock failure processes is of great significance for the prevention and control of engineering geological disasters [14]. Acoustic emission is the phenomenon of strain energy released in the form of elastic waves from microcracking behaviors within rocks [15,16]. Parametric features (count, peak amplitude, rise time, duration, energy, entropy, peak frequency, etc.) can be obtained from the acoustic emission spectrum and waves [17,18], which provide information for identifying microcracking behaviors during the deformation process of rocks. It has been proven that the acoustic emission parameters extracted from the detected acoustic emission waves are closely related to the evolution of fatigue damage [19–21]. Among them, the RA-AF crack classification criteria are widely used in understanding the failure mode [22], and the development process of cracks in different stages during the deformation process of rocks can be obtained by calculating the number or proportion of crack signals [23,24]. Zhao et al. [25] analyzed the differences in the types of cracks when sandstone exhibits different fracture modes, indicating that specimens characterized by shear failure have more shear crack acoustic emission signals during deformation.

The study of rock behavior under cyclic loading originated in mining science [26] and has extensively incorporated oil and natural gas storage [27,28], pumped storage power plants [29], slopes [30], tunnels [31], and other fields. Laboratory studies of cyclic loading can be roughly divided into two categories based on the load form and research purpose. One category involves determining the fatigue limit of rocks through constant-amplitude cyclic loading [32,33]; the other category uses increased mean stress and amplitude to study the rock damage evolution [34] and mechanical parameters [35]. This type of cyclic loading experiment is called a damage-controlled test [36]. Future sustainable energy systems need to be equipped with integrated energy storage technologies, such as pumped storage and compressed-air energy storage. In these projects, the surrounding rock will bear complex forms of cyclic loading. It is difficult to study the mechanical responses of rocks in different stress stages through monotonic loading tests. Therefore, in this study, a cyclic damage-controlled experiment was used to study the mechanical responses and acoustic emission characteristics of brittle rocks in different stress stages. Firstly, the pre-peak crack thresholds of two kinds of granite were determined. On this basis, the typical characteristics of the two kinds of granite in different stress stages were studied through a cyclic loading test with crack thresholds as the stress boundaries.

2. Experimental Materials and Procedures

2.1. Experimental Samples

The two granites used in this study were taken from Zhen'an in Shaanxi Province and Rizhao in Shandong Province, China. They are gray and light brown, respectively, and both are compact massive structures. The microstructures and energy spectrum analyses of the two granites are shown in Figure 1. It can be seen from the figure that there are obvious differences in the microstructure and mineral elements between the two kinds of granite. The MTS815 Flex Test GT rock mechanics experimental system was used in the experiment, as shown in Figure 2. This system can measure the axial and radial deformation of the specimen in real time and record the load, stress, displacement, and strain values. According to the method recommended by the International Society of Rock Mechanics (ISRM), the two granites were loaded in a cylinder with a diameter (D) of 50 mm and a height (H) of 100 mm. Before the test, the appearance of the processed rock samples was carefully observed to confirm that there were no obvious weak surfaces, such as joints or cracks.

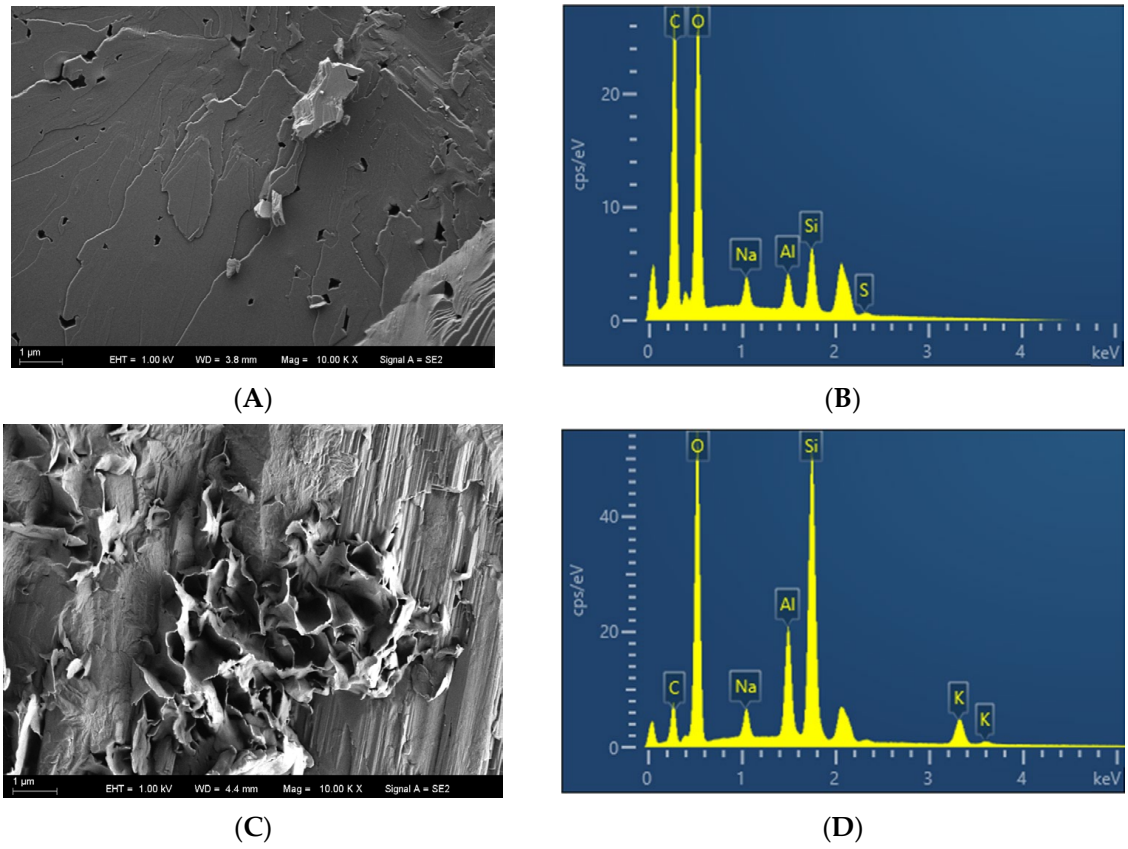

Figure 1. The two types of granite used in the experiment. (**A**) Scanning electron microscopy (SEM) image of the Zhen'an granite. (**B**) Energy spectrum of the Zhen'an granite. (**C**) SEM image of the Rizhao granite. (**D**) Energy spectrum of the Rizhao granite.

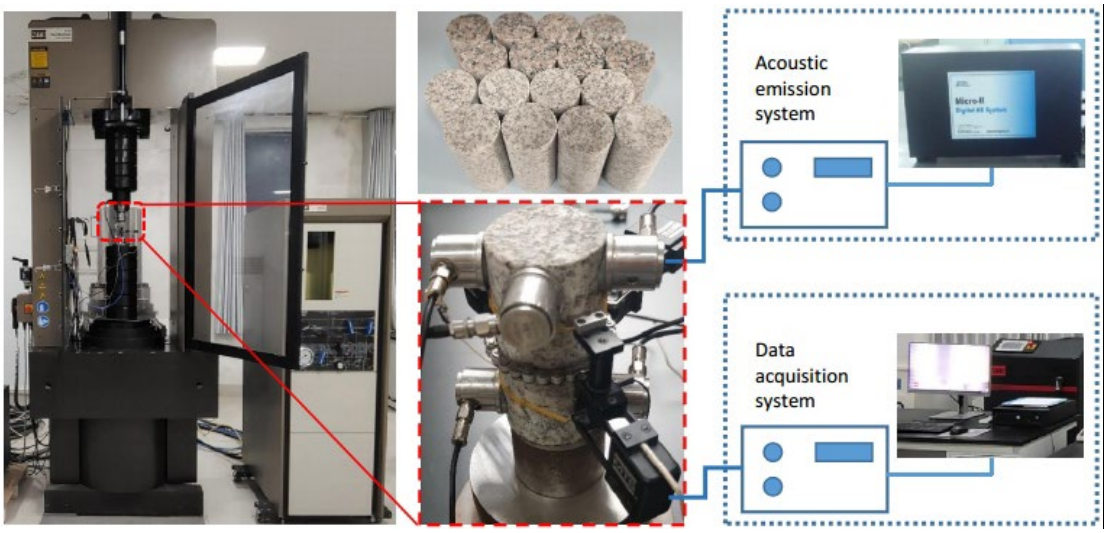

Figure 2. Rock sample and experimental equipment.

2.2. Crack Thresholds of the Two Types of Granite

Stress stages are categorized according to the characteristic crack threshold, and the study of stress stages is based on the accurate selection of the crack threshold. Crack damage stress can be determined using the maximum point of the total volumetric strain [1]. Martin and Christiansson [9] proposed that the determination of the crack closure threshold and the crack initiation threshold can be carried out using the relationship between the crack

volumetric strain and the axial strain, as shown in Figure 3. The elastic volumetric strains (ε_v^e) and crack volumetric strains (ε_v^p) of cylindrical specimens can be obtained using the following equations:

$$\varepsilon_v^e = \frac{1-2\nu}{E}(\sigma_1 + 2\sigma_3) \quad (1)$$

$$\varepsilon_v^p = \varepsilon_v - \varepsilon_v^e \quad (2)$$

where ν and E are the Poisson ratio and elastic modulus obtained according to the linear elasticity stage, respectively.

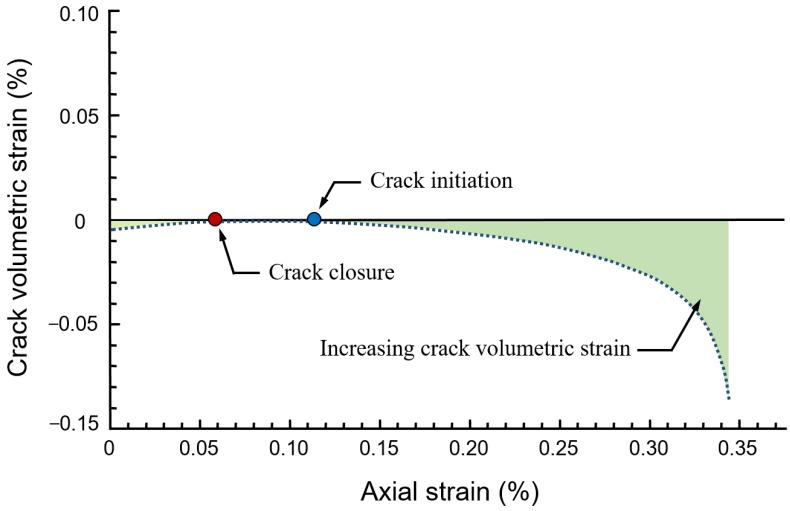

Figure 3. Determination of crack closure stress and crack initiation stress in rocks using the crack volumetric strain.

The pre-peak crack thresholds of the two kinds of granite were measured. Two to three groups of experiments were carried out for each kind of granite. The average crack thresholds obtained are shown in Table 1.

Table 1. Average crack thresholds of the two kinds of granite.

Crack Threshold	Mean Value (MPa)	
	Zhen'an Granite	Rizhao Granite
Crack closure threshold σ_{cc}	40	31
Crack initiation threshold σ_{ci}	45	47
Crack damage threshold σ_{cd}	96	89
Peak strength σ_f	160	139

2.3. Experimental Scheme

To further explore the use of cyclic loading in order to study the mechanical properties of rocks under certain stress levels, cyclic loading using the crack threshold as the limit was conducted on the two granite specimens during the four pre-peak stages: crack closure, linear elastic deformation, crack initiation and stable crack growth, and crack damage and unstable crack growth. The crack thresholds used in the experiment are shown in Table 1. Due to the differences between the rock samples, in order to prevent the specimens from rapidly failing when the strength neared its peak, according to the pre-experimental results, the load amplitude in the crack damage and unstable crack growth stage was reduced, and the corresponding peak strength was reduced by 5 MPa. The loading rate in the experiment was fixed at 10 kN/s. The stress path is shown in Figure 4. Three groups of experiments were carried out for each kind of granite. AE data acquisition was carried out using a PCI-II AE testing system from Physical Acoustics Corporation (PAC), Princeton Junction, NJ, USA.

The signals obtained from the AE sensor were amplified with a gain of 40 dB to filter the background noise, and the AE trigger threshold was set to 40 dB for each test. The main operating frequency range of the AE sensor used in the experiment is 35–100 kHz, and the resonant frequency is about 55 kHz.

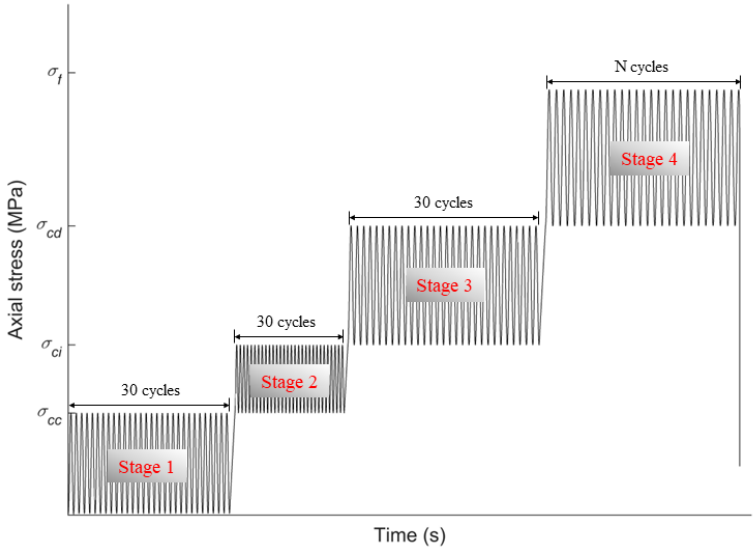

Figure 4. Stress path of the experiment.

3. Analysis of Experimental Results

3.1. Strain Characteristics

Figures 5 and 6 show the stress-strain curves of the two granites during the experiment. During the crack closure stage, the granite specimens mainly underwent compressive deformation along the axial direction, the lateral tensile deformation was small, and the specimen's volume was compressed. In the first few cycles of this stage, the specimen showed obvious irreversible deformation. This shows that, unlike the results obtained by Alkan et al. [37] in a triaxial compression test of rock salt, the crack closure process of granite is irreversible.

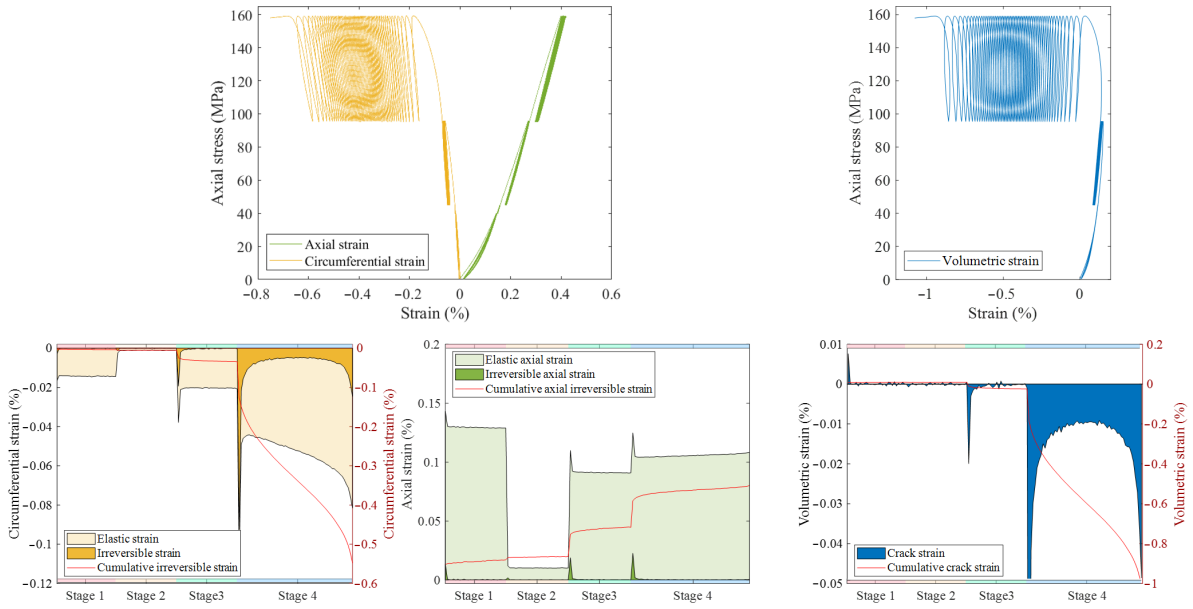

Figure 5. Axial, lateral, and volumetric stress-strain relationships, and the elastic and plastic strains of the axial, lateral, and volumetric strains induced by a single cyclic load (Zhen'an granite).

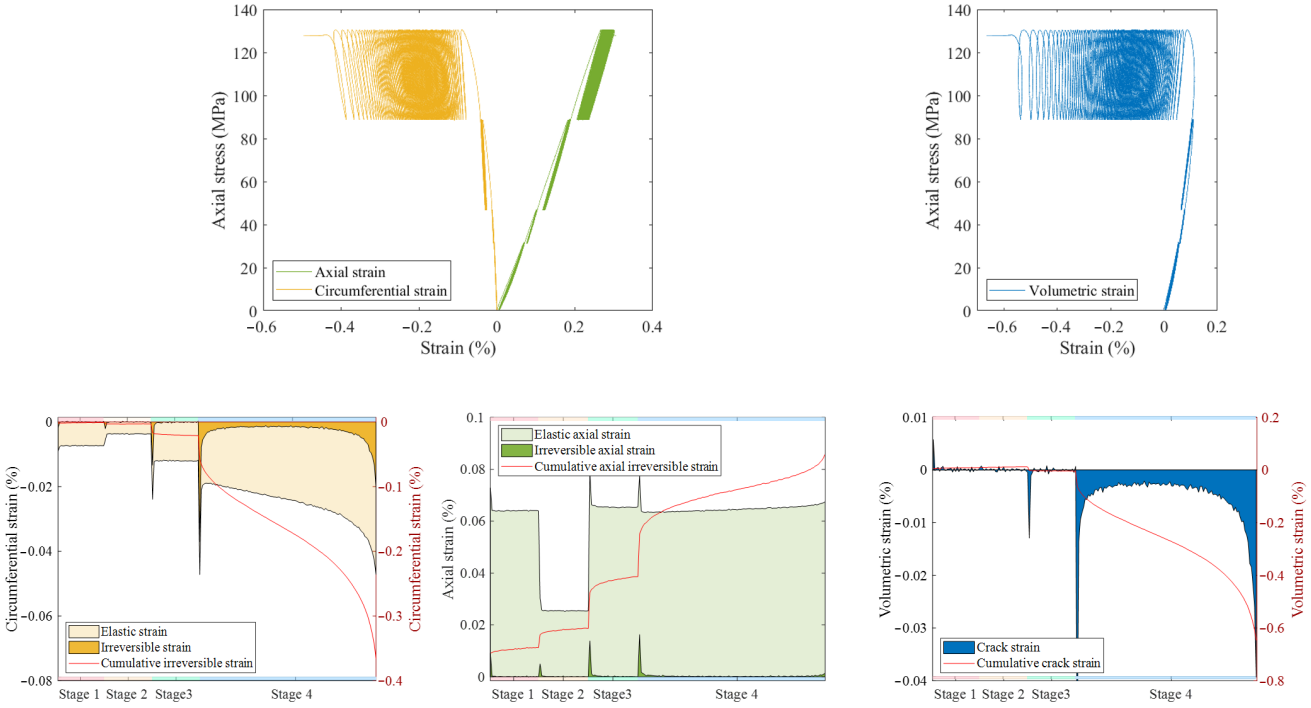

Figure 6. Axial, lateral, and volumetric stress-strain relationships, and the elastic and plastic strains of the axial, lateral, and volumetric strains induced by a single cyclic load (Rizhao granite).

Because the rock is not an ideal elastoplastic material and the linear elastic deformation stage is not completely elastic, the specimen underwent low-level axial compression and lateral expansion under loading. In addition, the rock sample underwent a certain axial and lateral expansion after the initial cycle. However, the specimen's crack volumetric strain was essentially 0.

During the crack initiation and stable crack growth stage, irreversible axial and lateral deformation mainly occurred during the initial cycle under this stress level. The irreversible axial and lateral deformation generated during a single cycle gradually became 0 as the number of cycles increased, and the corresponding specimen underwent gradual and stable volume expansion, indicating that rock fracturing under cyclic loads below the crack damage threshold can converge to a fixed level. In addition, the crack propagation in this stage can be controlled using the load's magnitude.

During the crack damage and unstable crack growth stage, the specimen underwent a certain irreversible circumferential and volumetric deformation after each loading and unloading process. As the number of cycles increased, the hysteresis curves of the circumferential and volumetric strains could be divided into three processes: (1) during the first several loading and unloading cycles, the hysteresis curve was sparse; (2) then, the hysteresis curve remained dense, and irreversible deformation accumulated at an almost constant rate; and (3) finally, when the damage accumulated to a certain level, the hysteresis curve became very sparse again until the specimen failed. In this stage, irreversible circumferential and volumetric deformation continuously accumulated, resulting in irreversible deformation that was several times that of the previous three stress stages.

Irreversible deformation is the main macroscopic manifestation of rock damage, and thus the irreversible deformation compliance $C^p_{(i,j)}$ was introduced to evaluate the development of rock damage in each stage. The irreversible deformation compliance is expressed as follows:

$$C^p_{(i,j)} = \frac{\Delta\varepsilon^p_i}{\Delta\sigma_j} \quad (3)$$

where ε_i denotes the irreversible axial, lateral, and volumetric deformation caused by the initial loading and unloading cycle in each stress stage, and $\Delta\sigma_j$ represents the difference between the cyclic load's upper and lower limits in each stress stage.

The $C^p_{(i,j)}$ of the two granite specimens in the different stress stages is shown in Figure 7. Irreversible axial deformation involves the superposition of the closure and the development of cracks inside the specimen along the axial direction. The irreversible axial deformation compliance $C^p_{(a,j)}$ changed slightly in the different stress stages, indicating that the limited axial load caused the granite specimens to essentially exhibit the same rate of damage along the axial direction in the different stress stages. Compared to $C^p_{(a,j)}$, the irreversible circumferential deformation compliance $C^p_{(c,j)}$ can better reflect the rock damage development process. The $C^p_{(c,j)}$ values corresponding to the four pre-peak stages were all less than 0, and the absolute value increased nonlinearly, indicating that the development speed of the internal cracks along the circumferential direction increased significantly as the load level increased. The irreversible volumetric deformation compliance $C^p_{(v,j)}$ was positive during the crack closure stage; meanwhile, it was essentially 0 during the linear elastic deformation stage, and it was significantly reduced during the subsequent stages. These observations show that the rock's internal cracks changed from closed to open under the load, and the rock's overall damage rate also significantly increased.

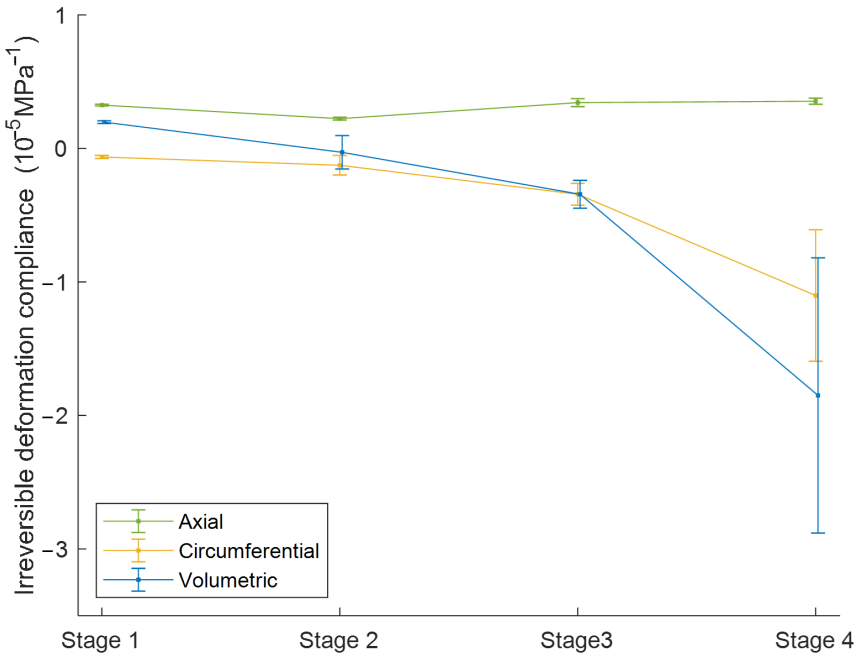

Figure 7. Irreversible deformation compliance in the different stress stages.

3.2. Nonlinear Hysteresis

The stress-time and strain-time curves were normalized. According to the previous division of the stress stages, the typical curves of each stress stage are shown in Figures 8 and 9. The normalization formulas are as follows:

$$V_\sigma = \frac{\sigma - \sigma_{\min}}{\sigma_{\max} - \sigma_{\min}} \tag{4}$$

$$V_\varepsilon = \frac{\varepsilon - \varepsilon_{\min}}{\varepsilon_{\max} - \varepsilon_{\min}} \tag{5}$$

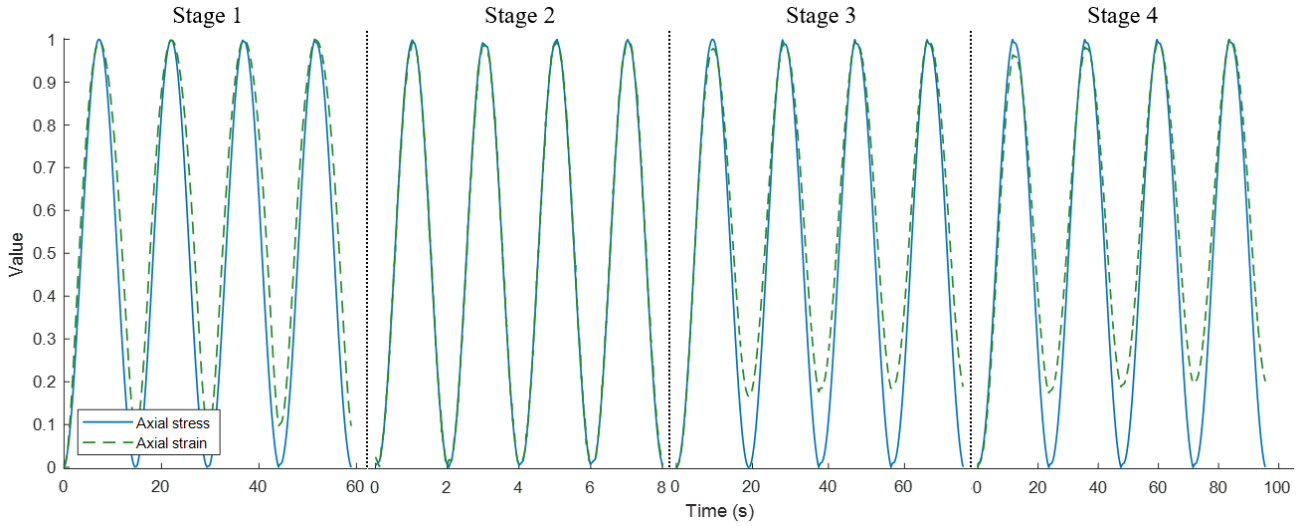

Figure 8. Stress-time and axial strain-time curves of the granite specimens.

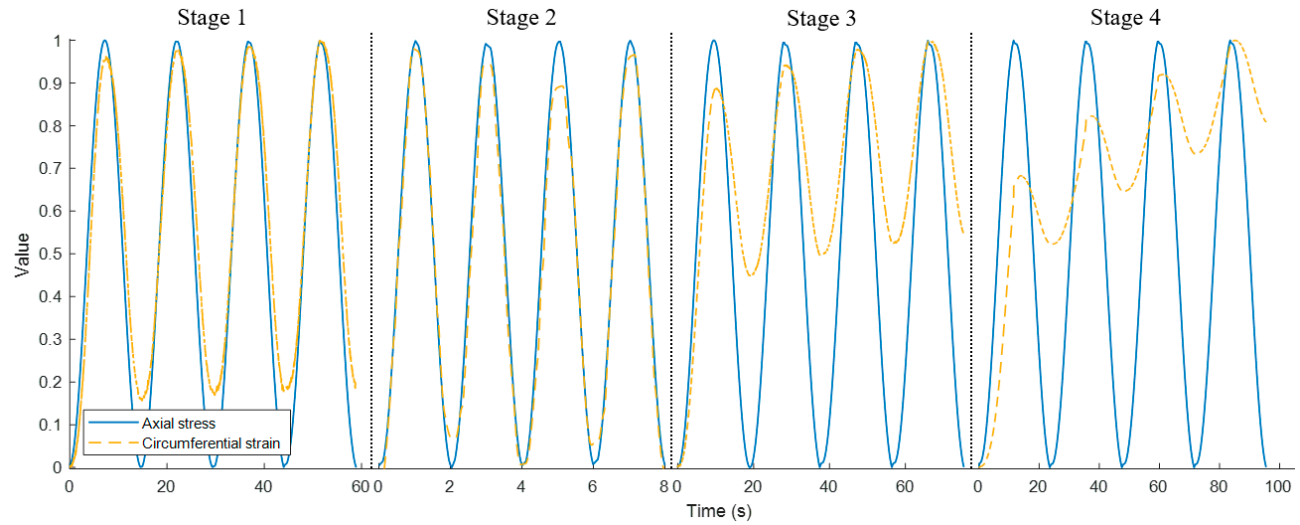

Figure 9. Stress-time and circumferential strain-time curves of the granite specimens.

The inhomogeneity and multicomponent characteristics caused the rock's unique hysteresis. During the linear elastic deformation stage, both the axial and circumferential strain phases were essentially the same as the stress phase, indicating that the granite is significantly linearly elastic in this stage. During the stages of crack closure, crack initiation, and crack damage and unstable crack growth, the axial strain phase led the stress phase during the loading process and lagged the stress phase during the unloading process. The circumferential strain increased with the number of cycles due to the influence of the irreversible circumferential deformation, and the circumferential strain phase lagged the stress phase during both the loading and unloading processes.

There may be a leading, equal, or lagging relationship between the strain phase and stress phase, and the relationship between the two is mainly affected by two factors. The first is the viscosity of the liquid between the mineral particles and the friction between the interfaces. Because the stress has an impact on these phenomena, the hysteresis effect that they cause is significantly correlated with the load's magnitude. During the initial loading stage, the load is relatively small, the pore pressure and the normal force between the contact surfaces are also relatively small, the liquid viscosity and friction between the interfaces are relatively weak, and the specimen's strain rate is relatively large. As the load increases, the squeezing effect between the mineral particles gradually increases, and the

liquid viscosity and friction between the interfaces also increase, resulting in a gradual slowdown in the specimen's strain rate. Therefore, the strain rate is first large and then small, which results in the strain phase leading in the strain-time curve. In contrast, during the unloading process, the strain rate is first small and then large, which results in the strain phase lagging in the strain-time curve. The second factor is irreversible deformation of the rock. This irreversible deformation changes the initial position of the strain under cyclic loading, thereby affecting the relationship between the strain phase and stress phase. Figure 10 shows the effect of the above two factors on the phase change.

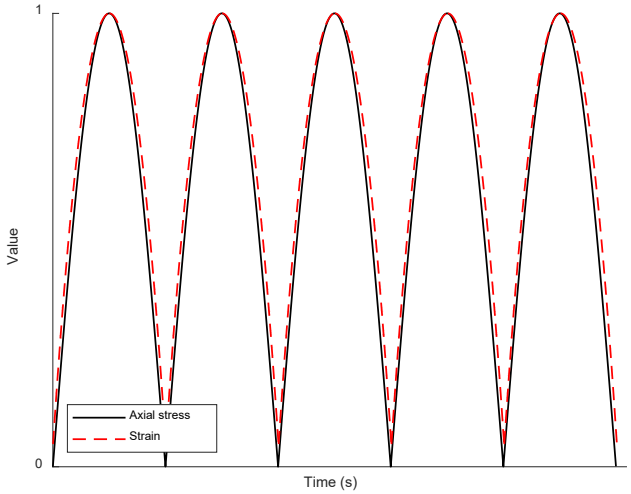

(**A**)

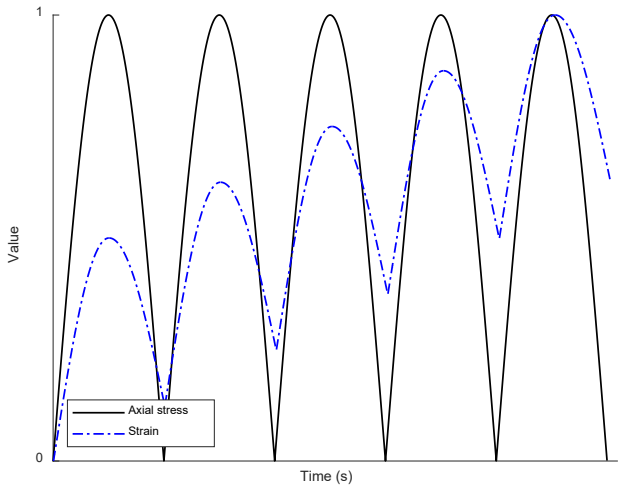

(**B**)

Figure 10. Two influencing factors of the strain phase. (**A**) Effect of hysteresis caused by liquid viscosity and interfacial friction on the strain phase. (**B**) Effect of irreversible deformation on the strain phase.

Elastic deformation and irreversible deformation occur simultaneously any time a rock is under a load, and the proportions of the two are different in different stages, resulting in a difference in the relationship between the strain phase and stress phase in different stages. Because the irreversible axial deformation is relatively small, the liquid viscosity and interfacial friction are the dominant factors that govern the relationship between the axial strain phase and the stress phase. Therefore, during the stages of crack closure,

crack initiation, and crack damage and unstable crack growth, the overall manifestation of the granite samples' phase was as follows: the axial strain phase led during the loading process, and the axial strain phase lagged during the unloading process. The irreversible lateral deformation was relatively large, and the liquid viscosity, interfacial friction, and irreversible deformation together constituted the relationship between the lateral strain phase and the stress phase. During the stages of crack closure, crack initiation, and crack damage and unstable crack growth, as the specimen's stress level gradually increased, the distance between the mineral particles gradually decreased, resulting in increases in the liquid viscosity and interfacial friction and, in turn, an increased hysteresis effect caused by the liquid viscosity and interfacial friction; therefore, hysteresis of the circumferential strain occurred in the following order: crack closure < crack initiation < crack damage and unstable crack growth.

3.3. Energy Evolution

As shown in Figure 11, there was residual strain in the rock after unloading in the cyclic loading experiment, as indicated by the noncoincidence of the loading and unloading curves. The area under the stress-strain curve during the loading stage is the total energy density U_i generated by the external force; the area under the stress-strain curve during the unloading stage is the elastic strain energy density U_i^e, which can be released inside the rock; and the difference between U_i and U_i^e is the dissipated energy density U_i^d of the rock's internal damage or plastic deformation loss. If there is no heat exchange between the rock sample and the outside world during the experiment (the total energy of the rock remains unchanged in an isolated system), U_i^e and U_i^d can be calculated using the following equations [38]:

$$U_i^e = \int_{\varepsilon''}^{\varepsilon'} \sigma_i \mathrm{d}\varepsilon_i \tag{6}$$

$$U_i^d = \int_0^{\varepsilon'} \sigma_i \mathrm{d}\varepsilon_i - \int_{\varepsilon''}^{\varepsilon'} \sigma_i \mathrm{d}\varepsilon_i \tag{7}$$

where ε' is the axial strain corresponding to the end of loading, and ε'' is the axial strain corresponding to the end of unloading.

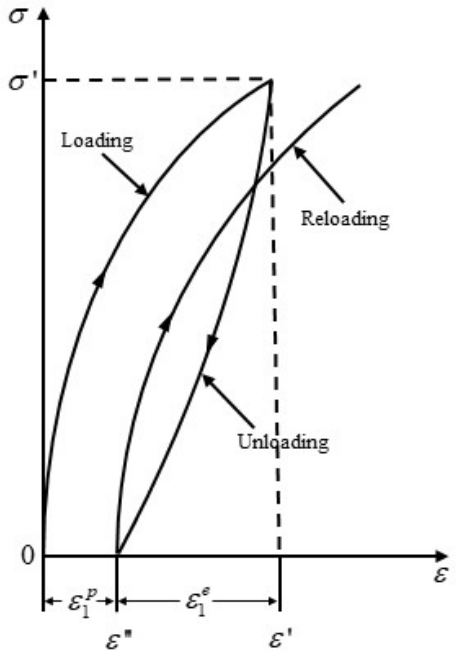

Figure 11. Energy per unit volume in the loading and unloading curves at stress level σ′.

According to the uniaxial cyclic loading and unloading stress-strain curves, the variation patterns of the two granites' total energy density, elastic energy density, and dissipated energy density in the different stress stages were obtained, as shown in Figures 12 and 13.

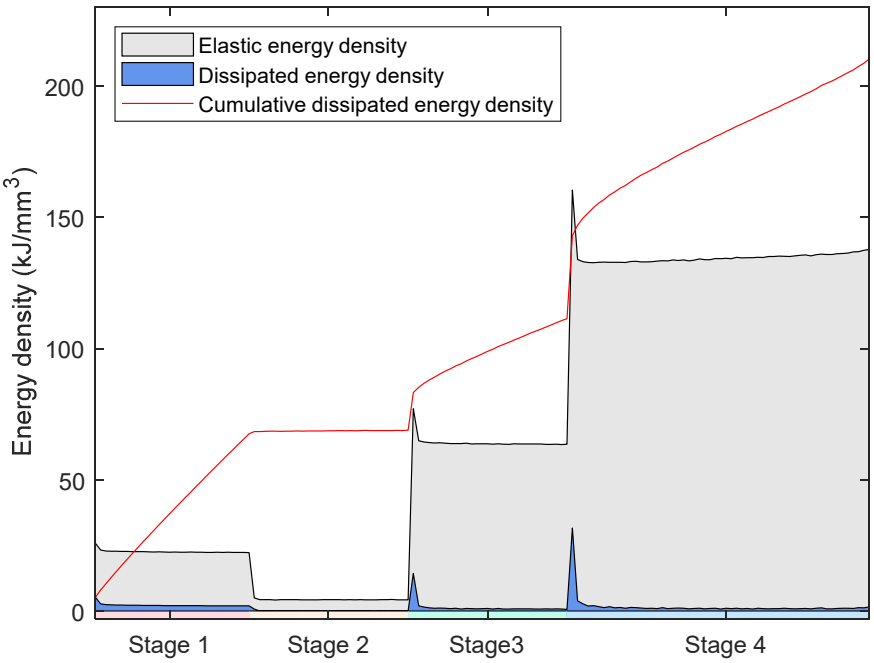

Figure 12. Total energy density, elastic energy density, and dissipated energy density of the Zhen'an granite in the different stress stages.

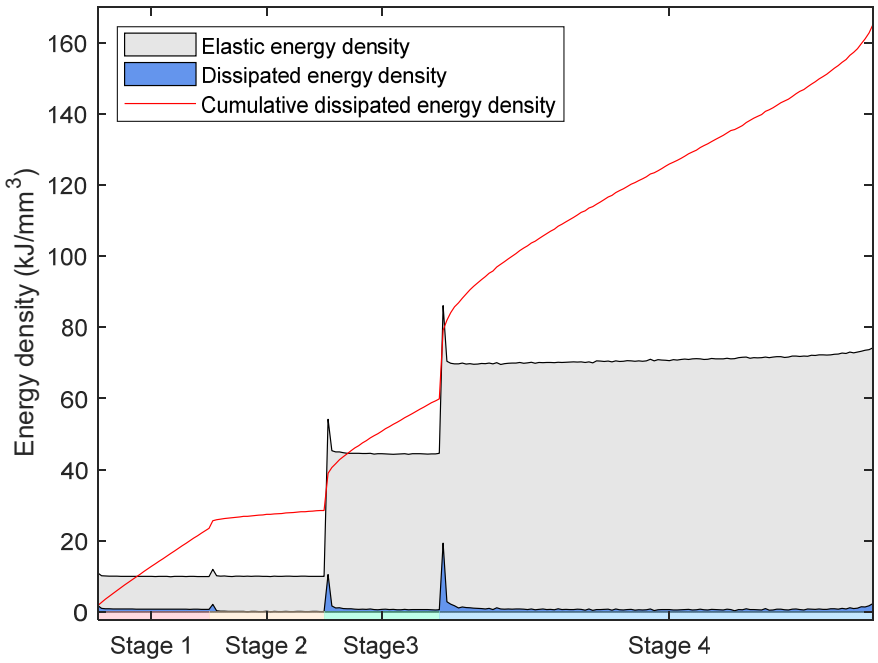

Figure 13. Total energy density, elastic energy density, and dissipated energy density of the Rizhao granite in the different stress stages.

The elastic energy, dissipated energy, and cumulative dissipated energy of the two granites in each stress stage had similar characteristics. The energy dissipated during the crack closure stage provided the energy required to close the pores or microfractures within the rock, with each loading and unloading cycle creating fixed

dissipated energy. In addition, the cumulative dissipated energy increased linearly with the number of cycles. During the linear elastic deformation stage, the work conducted by the testing machine on the rock sample was almost completely converted into elastic energy stored in the rock sample, and the dissipated energy was essentially 0. During the crack initiation and stable crack growth stage, the dissipated energy was relatively large during the first few cycles and gradually decreased as the number of cycles increased, finally approaching zero. In the initial stage of crack damage and unstable crack growth, the dissipated energy generated during a single loading and unloading cycle gradually decreased. As the elastic energy was released and the dissipated energy increased, the accumulation of irreversible deformation in the loaded rock sample triggered a reduction in the rock sample's energy storage properties, and the dissipated energy increased significantly during the several cycles that occurred when the rock was close to failure.

3.4. Crack Propagation Evolution

AE activity in rocks is the result of dislocation movement, grain boundary migration, or microcrack closure, initiation, propagation, and merging. AE source localization is an effective means of characterizing the damage evolution during rock loading, since it allows the damage and crack evolution throughout the loading process to be continuously visualized in time and space. In general, if the rock's wave velocity is known and constant, then at least (n − 1) sensors are needed for an n-dimensional problem [39]. To obtain a better localization, a total of six sensors were used in this experiment, with three sensors arranged at the upper and lower ends on a horizontal plane 5 mm away from the ends, as shown in Figure 14.

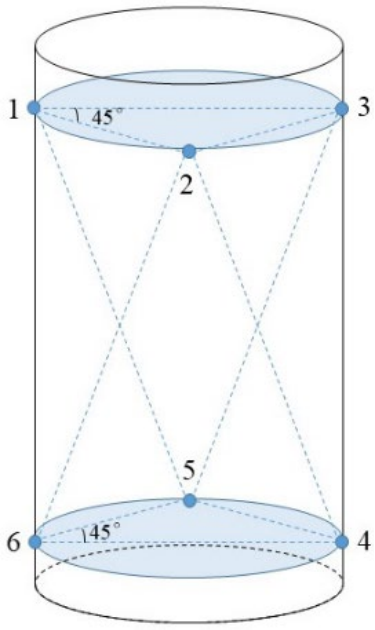

Figure 14. Schematic diagram of the AE sensor layout.

Figures 15 and 16 show the spatial distribution patterns of the AE events in the different stages. In the figures, the AE events are drawn as spheres. A sphere's size represents the AE event's level of energy, and the sphere's color (from purple to red) represents the order in which the AE events occurred. Since there are dense acoustic emission events in the stage of crack damage and unstable crack growth, this stage was divided into three parts according to the same time interval.

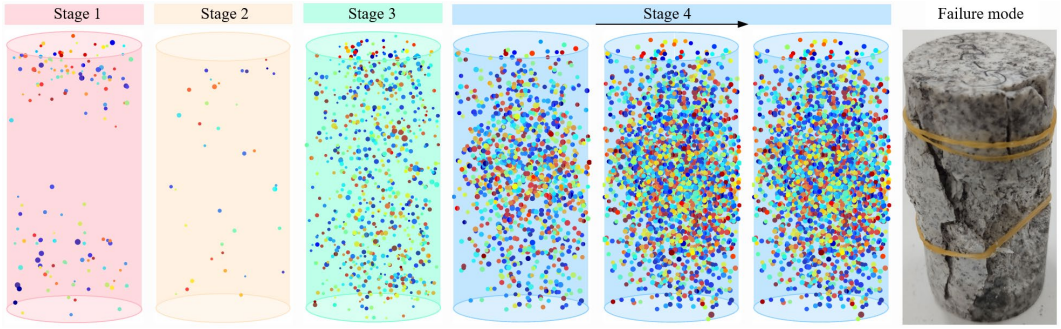

Figure 15. Spatial distribution patterns and failure mode of AE events in the different stress stages (Zhen'an granite).

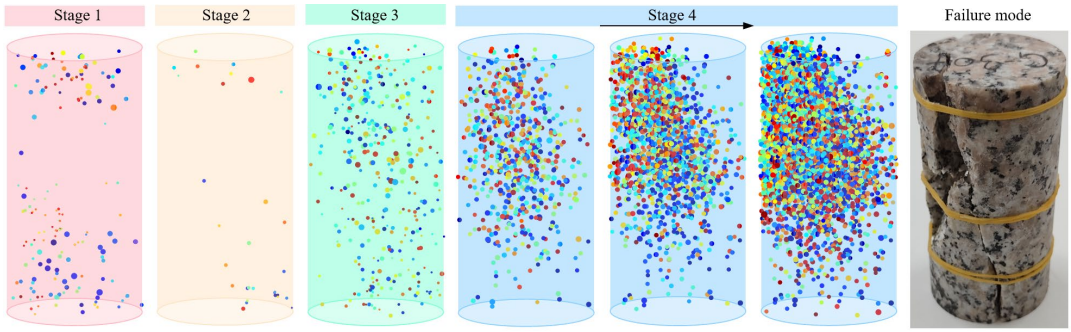

Figure 16. Spatial distribution patterns and failure mode of AE events in the different stress stages (Rizhao granite).

The spatial distribution patterns of the AE events in each stress stage had their own characteristics. During the crack closure stage, due to the friction of the crosshead, the AE events were mainly distributed at the top and bottom of the rock sample, and there were fewer AE events in the middle. At the same time, the energy of the AE events that occurred during the initial stage of loading was significantly greater than that of the subsequent AE events. This phenomenon correlates with the conclusion in Section 3.1 that irreversible deformation occurs mainly during the initial loading and unloading, suggesting that crack closure and pore compaction in this stage occur mainly during the initial loading but that compaction still occurs during the subsequent cycles. During the linear elastic deformation stage, the specimens were dominated by the matrix's elastic deformation, there was no obvious internal damage, and the AE events were sparse. However, AE events during the crack initiation and stable crack growth stage occurred throughout the whole specimen. In particular, the AE events were almost evenly distributed, indicating that crack initiation occurred randomly in this stage and that there was no connection between the microcracks. The AE events during the crack damage and unstable crack growth stage gradually transformed from a random disordered pattern during the previous stage to a localized order. The time sequence shows that there was obvious aggregation of AE events early during this stage, and the subsequent cycles only caused the AE events to become denser, showing that many cracks appeared in the rock, which were connected to each other and eventually formed a macroscopic failure surface in the sample.

When studying the strength of metal materials, it is often found that the peak RMS value of AE signals occurs near the yield point. Figures 17 and 18 show the AE count and average RMS value of the granite samples during a single cycle with a loading process. In the cyclic loading test of the granites, there were no obvious characteristics of the RMS value before failure, but there were differences in the characteristics in the different stress stages. In the stage of crack damage and unstable crack growth, the RMS value significantly increased compared to that in the first three stages, corresponding to a strong dislocation inside the material. The AE count is closely related to the development of cracks in the

interior of rocks, and an increase in its value indicates an acceleration in the rate of rock damage. In the initial stage of loading, the rock was in the crack closure stage, and new cracks had not yet been generated, resulting in relatively low acoustic emission ringing counts. There was no significant crack propagation inside the rock during the linear elastic deformation stage, and the AE count was essentially zero. The AE count in the crack initiation and stable crack growth stage gradually decreased as the cyclic loading progressed. Overall, in the first three stages, when the load exceeded the maximum stress value of the previous level, the AE count increased significantly, but it gradually decreased during the subsequent cycles at the same load level, which demonstrates the existence of a significant Kaiser effect. When the magnitude of the cyclic load reached the stress threshold in the stage of crack damage and unstable crack growth, the ringing count of the specimen per cycle was large, the acoustic emission information was intensive, damage constantly accumulated, and plastic deformation developed rapidly until the specimen failed.

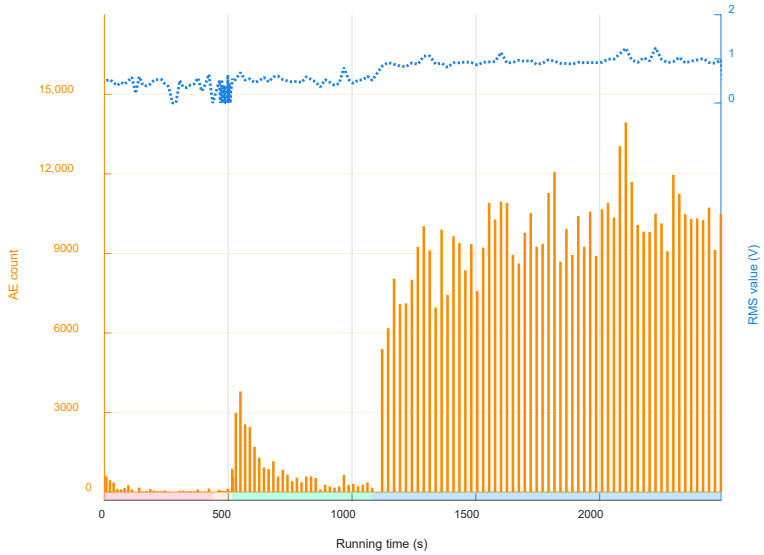

Figure 17. Changes in the AE count and average RMS value of the granite samples during a single cycle with a loading process (Zhen'an granite).

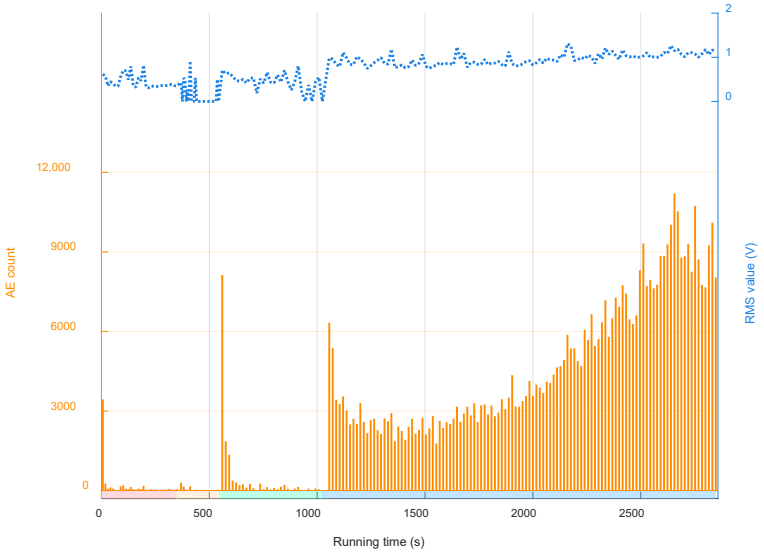

Figure 18. Changes in the AE count and average RMS value of the granite samples during a single cycle with a loading process (Rizhao granite).

Two AE parameters, namely the ratio of the rise time to the amplitude (RA) and the average frequency (AF), can reflect the type of cracks inside the rock [40,41]. The RA value is the ratio of the rise time to the amplitude, and the AF is obtained from the ratio of the ringing count to the duration. For tensile cracks, the elastic energy is released instantaneously, so the rise time and duration are short, the amplitude is large, and the ringing count is large. Therefore, the RA value is small, and the AF value is large. Shear cracks, on the other hand, exhibit the opposite pattern.

$$\mathrm{AF} = \frac{\text{AE count}}{\text{AE duration}} \tag{8}$$

$$\mathrm{RA} = \frac{\text{AE rise time}}{\text{AE amplitude}} \tag{9}$$

According to the Japanese JCMS-III B5706 (2003), which is the monitoring method for active cracks in concrete using AE [42], the slope of the dividing line in Figure 19 is defined as k, where signals with AF/RA < k are defined as shear crack signals, and signals with AF/RA > k are defined as tensile crack signals. Ohno and Ohtsu [43] found that the classification of crack types with k = 80 was close to the results obtained through Simplified Green's functions for Moment tensor Analysis (SiGMA). Gan et al. [44] used k = 90, and the RA-AF determination result was the closest to the inversion result of the moment tensor; their study also demonstrated that the k estimated from the whole process was applicable during all loading phases.

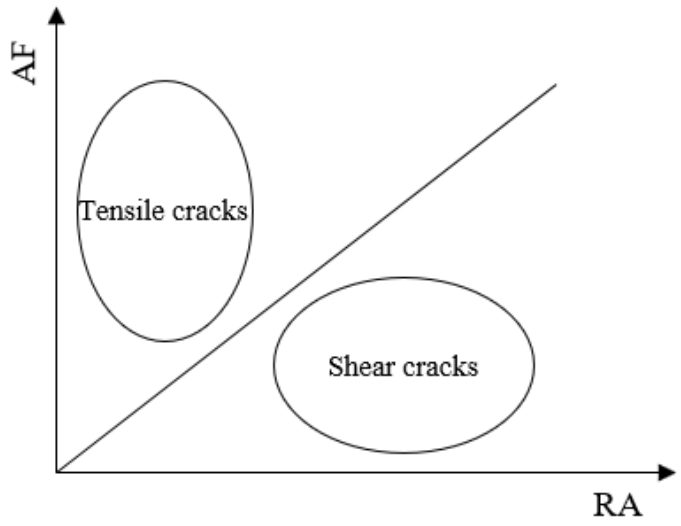

Figure 19. Fracture mechanism determination based on the RA and AF values.

The distribution of tensile and shear cracks in the granites was studied in advance, with k equal to 85, 90, and 95. The results showed that, when k was taken between 85 and 95, the value of k had little effect on the proportion of tensile and shear cracks. Therefore, subsequent studies were conducted under the condition of k being equal to 90. Figures 20 and 21 show the distribution of the two types of granites' RA and AF values in the different stages. During the crack closure stage, the AE events were distributed in both the tensile and shear crack regions, with the AF concentrated in the range of 0–100 kHz and the RA concentrated in the range of 0–5 ms/V. During the linear elastic deformation stage, the number of AE events was relatively small, and most of the cracks were tensile cracks. During the crack initiation and stable crack growth stage, the number of AE events began to gradually increase; the AF was concentrated in the range of 0 to 125 kHz, the RA was distributed in the range of 0 to 20 ms/V, and the percentage of shear cracks increased. During the crack damage and unstable crack growth stage, AE events were active, the

RA was widely distributed in the range of 0–40 ms/V, and the number of shear cracks increased; however, the proportion of shear cracks was still lower than that of tensile cracks. Overall, for the two granites, the cracks generated in each pre-peak stage were all tensile and shear cracks, and the tensile cracks were dominant.

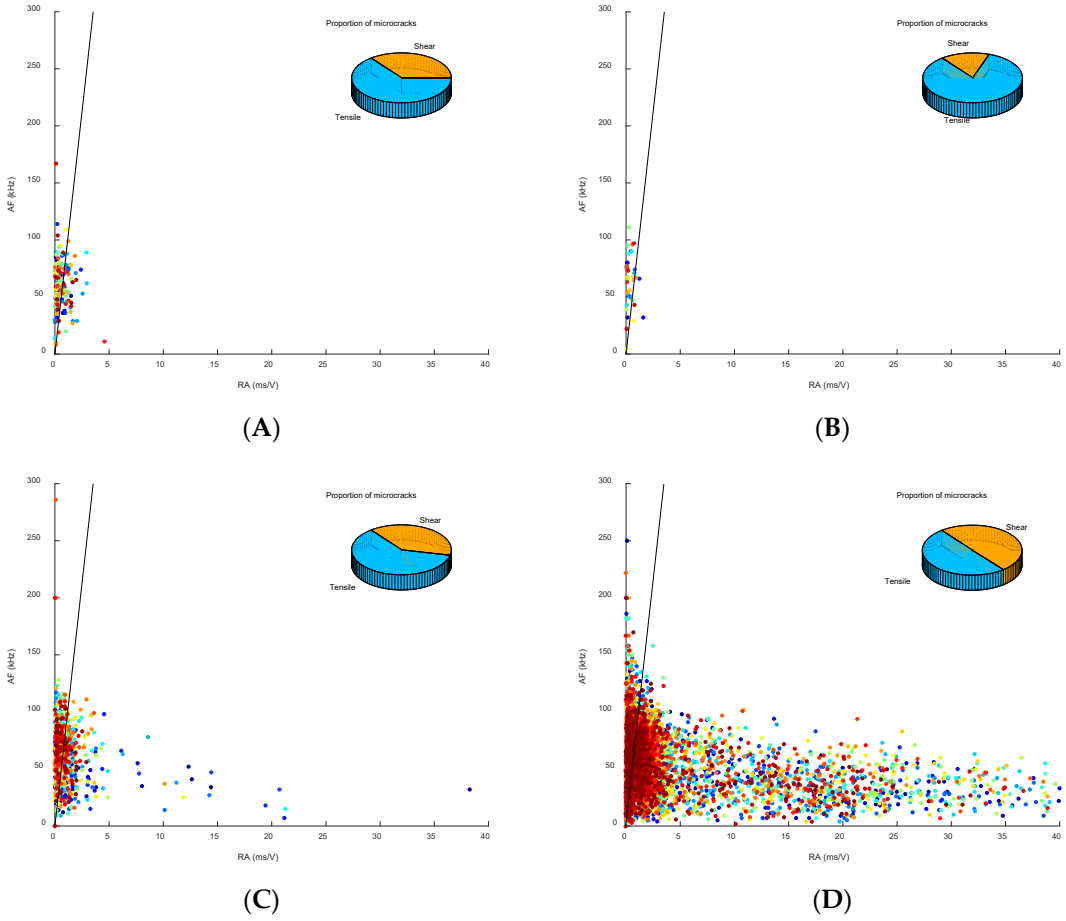

Figure 20. RA-AF evolution of the Zhen'an granite. (**A**) Stage of crack closure. (**B**) Stage of linear elastic deformation. (**C**) Stage of crack initiation and stable crack growth. (**D**) Stage of crack damage and unstable crack growth.

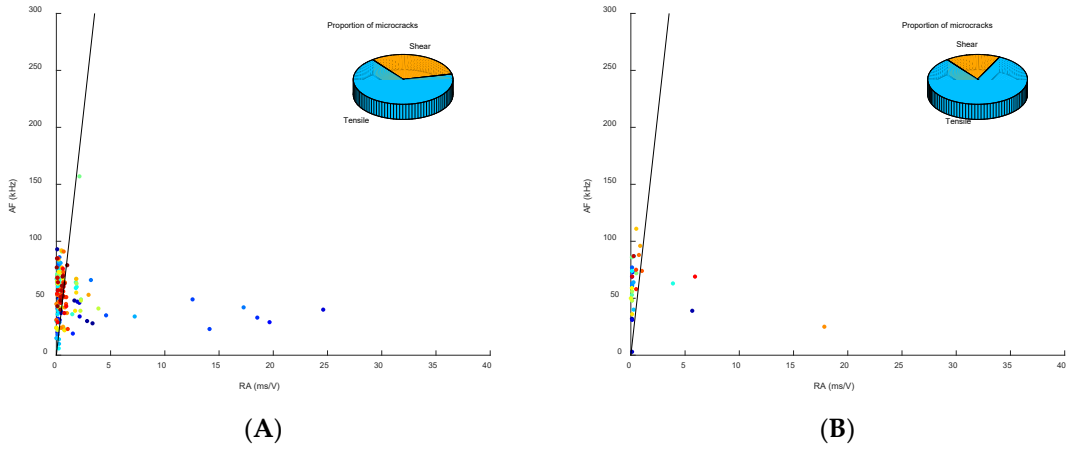

Figure 21. *Cont.*

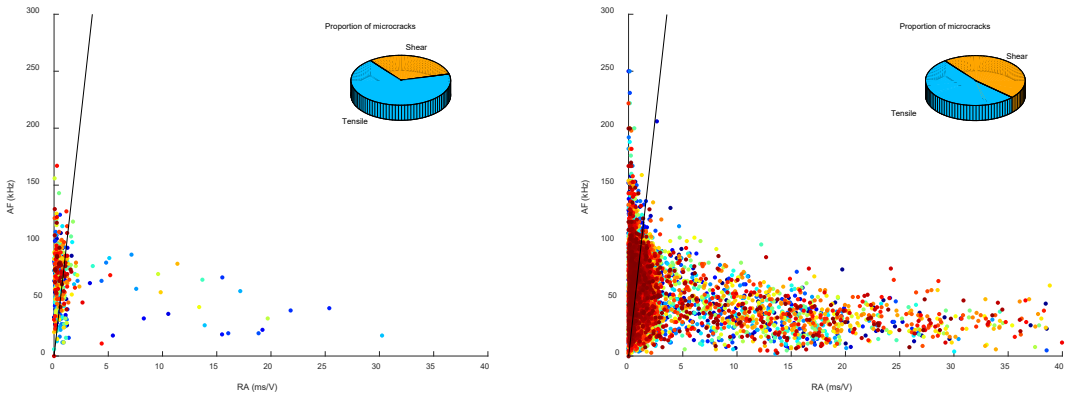

(**C**) (**D**)

Figure 21. RA-AF evolution of the Rizhao granite. (**A**) Stage of crack closure. (**B**) Stage of linear elastic deformation. (**C**) Stage of crack initiation and stable crack growth. (**D**) Stage of crack damage and unstable crack growth.

4. Discussion

In contrast to conventional cyclic loading, the experiments conducted in this study emphasize the objectivity and accuracy in setting the cyclic stress amplitude. The variation pattern of these parameters can be regarded as a macroscopic statistical reflection of the microcrack evolution inside the rock. The crack evolution characteristics of the two granites in the different stress stages were significantly consistent. AE events with relatively high energy occurred at the beginning of the crack closure stage, and the ratio of shear cracks to tensile cracks was approximately 2:3. During the linear elastic deformation stage, the matrix's elastic deformation was dominant, and AE events were sparse; during the crack initiation and stable crack growth stage, AE events were uniformly distributed within the specimen, indicating that crack initiation occurs randomly, and the proportion of shear cracks increased. At the beginning of the crack damage and unstable crack growth stage, AE events showed obvious aggregation, while AE events during the subsequent cycles were denser, and the proportion of shear cracks further increased but was still lower than that of tensile cracks.

Rocks are multiphase, multicomponent, nonhomogeneous natural geological materials, and complex cracks, joints, and pores are distributed inside them, which makes their internal stress field very complex under loading. Therefore, when a rock is loaded beyond its stress history for the first time, a new round of microcrack adjustments inside the rock can be triggered. It is reasonable to speculate that the closure of old cracks and the development of new cracks within a rock under loading occur at every moment, and that the proportions of the two affect the rock's macroscopic mechanical properties. During the crack closure stage, the closure of rock cracks is greater than that during crack initiation, and the rock becomes compacted macroscopically. During the linear elastic deformation stage, crack closure and crack initiation are similar, and the rock macroscopically behaves as an approximate elastic body. During the crack initiation and stable crack growth stage, the crack initiation is greater than the crack closure, and the stress concentration causes local stress in the rock that is greater than the average stress calculated according to the apparent area. However, after many cycles, the rock reaches a new steady state after structural adjustment. During the crack damage and unstable crack growth stage, crack initiation dominates. After multiple structural adjustments, the rock cannot reach a new steady state, and a chain reaction occurs. The external load causes the rock's internal structure to adjust, but the adjusted structure still cannot bear the external load. Under this level of external load, the rock's internal damage gradually accumulates until the rock fails.

5. Conclusions

(1) Irreversible deformation mainly occurs when a rock is subjected to a load that exceeds its stress history for the first time. However, one monotonic load cannot completely release the rock's plastic deformation potential, which is particularly obvious during the crack damage and unstable crack growth stage.

(2) Due to the influences of the liquid viscosity, interfacial friction, and irreversible deformation, the overall manifestation of the granites' phase during the stages of crack closure, crack initiation, and crack damage and unstable crack growth was as follows: the axial strain phase led during the loading process, the axial strain phase lagged during the unloading process, and the hysteresis of the circumferential strain gradually increased.

(3) The dissipated energy of a single cycle is associated with the progression of damage or plastic deformation in the rock. In the stage of linear elastic deformation, there is essentially no energy dissipation. During the crack initiation and stable crack growth stage, the dissipated energy of a single cycle gradually decreases with the number of cycles. In the stage of crack damage and unstable crack growth, the dissipated energy of a single cycle first decreases and then increases with the increase in the number of cycles.

(4) In the studied granites, the proportion of shear cracks was lower than that of tensile cracks in the different stress stages. With the increase in cyclic loading, the proportion of shear cracks gradually increased, and AE events gradually occurred in a certain area.

Author Contributions: All authors contributed to the study conception and design. Material preparation, data collection and analysis were performed by J.W., H.Y. and Y.Z. The first draft of the manuscript was written by H.L. and J.W. and all authors commented on previous versions of the manuscript. All authors have read and agreed to the published version of the manuscript.

Funding: This study was supported by the National Key Research and Development Program (Grant No. 2019YFC1509704) and the National Natural Science Foundation of China (Grant No. U1704243).

Institutional Review Board Statement: Not applicable.

Informed Consent Statement: Not applicable.

Data Availability Statement: The datasets generated during and/or analysed during the current study are available from the corresponding author on reasonable request.

Conflicts of Interest: The authors declare no conflict of interest.

References

1. Brace, W.F.; Paulding, B.W., Jr.; Scholz, C. Dilatancy in the fracture of crystalline rocks. *J. Geophys. Res.* **1996**, *71*, 3939–3953. [CrossRef]
2. Bieniawski, Z.T. Mechanism of brittle rock fracture. Part I: Theory of the fracture process. *Int. J. Rock Mech. Min. Sci. Geomech. Abstr.* **1967**, *4*, 395–406. [CrossRef]
3. Cheng, H.; Zhou, X.; Zhu, J.; Qian, Q. The effects of crack openings on crack initiation, propagation and coalescence behavior in rock-like materials under uniaxial compression. *Rock Mech. Rock Eng.* **2016**, *49*, 3481–3494. [CrossRef]
4. Martin, C.D. The Strength of Massive Lac du Bonnet Granite around Underground Openings. Ph.D. Thesis, Department of Civil and Geological Engineering, University of Manitoba, Winnipeg, MB, Canada, 1993.
5. Eberhardt, E.; Stead, D.; Stimpson, B.; Read, R.S. Identifying crack initiation and propagation thresholds in brittle rock. *Can. Geotech. J.* **1998**, *35*, 222–233. [CrossRef]
6. Bridgman, P.W. Volume changes in the plastic stages of simple compression. *J. Appl. Phys.* **1949**, *20*, 1241–1251. [CrossRef]
7. Handin, J.; Hager, R.V., Jr.; Friedman, M.; Feather, J.N. Experimental deformation of sedimentary rocks under confining pressure: Pore pressure tests. *Aapg Bull.* **1963**, *47*, 717–755.
8. Andersson, J.C.; Martin, C.D.; Stille, H. The Äspö pillar stability experiment: Part II—Rock mass response to coupled excavation-induced and thermal-induced stresses. *Int. J. Rock Mech. Min. Sci.* **2009**, *46*, 879–895. [CrossRef]
9. Martin, C.D.; Christiansson, R. Estimating the potential for spalling around a deep nuclear waste repository in crystalline rock. *Int. J. Rock Mech. Min. Sci.* **2009**, *46*, 219–228. [CrossRef]
10. Cai, M. Practical estimates of tensile strength and Hoek–Brown strength parameter mi of brittle rocks. *Rock Mech. Rock Eng.* **2010**, *43*, 167–184. [CrossRef]
11. Palchik, V.; Hatzor, Y.H. Crack damage stress as a composite function of porosity and elastic matrix stiffness in dolomites and limestones. *Eng. Geol.* **2002**, *63*, 233–245. [CrossRef]

12. Peng, J.; Cai, M.; Rong, G.; Yao, M.D.; Jiang, Q.H.; Zhou, C.B. Determination of confinement and plastic strain dependent post-peak strength of intact rocks. *Eng. Geol.* **2017**, *218*, 187–196. [CrossRef]
13. Wen, T.; Liu, Y.; Yang, C.; Yi, X. A rock damage constitutive model and damage energy dissipation rate analysis for characterising the crack closure effect. *Geomech. Geoengin.* **2018**, *13*, 54–63. [CrossRef]
14. Fang, K.; Zhang, J.; Tang, H.; Hu, X.; Yuan, H.; Wang, X.; An, P.; Ding, B. A quick and low-cost smartphone photogrammetry method for obtaining 3D particle size and shape. *Eng. Geol.* **2023**, *322*, 107170. [CrossRef]
15. Yin, T.; Li, Q.; Li, X. Experimental investigation on mode I fracture characteristics of granite after cyclic heating and cooling treatments. *Eng. Fract. Mech.* **2019**, *222*, 106740. [CrossRef]
16. Niu, Y.; Zhou, X.P.; Zhou, L.S. Fracture damage prediction in fissured red sandstone under uniaxial compression: Acoustic emission b-value analysis. *Fatigue Fract. Eng. Mater. Struct.* **2020**, *43*, 175–190. [CrossRef]
17. Chai, M.; Hou, X.; Zhang, Z.; Duan, Q. Identification and prediction of fatigue crack growth under different stress ratios using acoustic emission data. *Int. J. Fatiq.* **2022**, *160*, 106860. [CrossRef]
18. Zhou, X.P.; Zhang, J.Z. Damage progression and acoustic emission in brittle failure of granite and sandstone. *Int. J. Rock. Mech. Min. Sci.* **2021**, *143*, 104789. [CrossRef]
19. Chai, M.; Lai, C.; Xu, W.; Song, Y.; Zhang, Z.; Duan, Q. Determination of fracture toughness of 2.25Cr1Mo0.25V steel based on acoustic emission technique. *Int. J. Press. Vessel. Pip.* **2023**, *205*, 104998. [CrossRef]
20. Zhang, Y.; Shi, J.; Zheng, J. A method of fracture toughness JIC measurement based on digital image correlation and acoustic emission technique. *Mater. Des.* **2021**, *197*, 109258. [CrossRef]
21. Triantis, D.; Loukidis, A.; Stavrakas, I.; Pasiou, E.D.; Kourkoulis, S.K. Attenuation of the Acoustic Activity in Cement Beams under Constant Bending Load Closely Approaching the Fracture Load. *Foundations* **2022**, *2*, 590–606. [CrossRef]
22. Yao, Q.; Chen, T.; Tang, C.; Sedighi, M.; Wang, S.; Huang, Q. Influence of moisture on crack propagation in coal and its failure modes. *Eng. Geol.* **2019**, *258*, 105156. [CrossRef]
23. Triantis, D. Acoustic emission monitoring of marble specimens under uniaxial compression. *Procedia Struct. Integr.* **2018**, *10*, 11–17.
24. Munoz-Ibanez, A.; Delgado-Martín, J.; Herbón-Penabad, M.; Alvarellos-Iglesias, J. Acoustic emission monitoring of mode I fracture toughness tests on sandstone rocks. *J. Pet. Sci. Eng.* **2021**, *205*, 108906. [CrossRef]
25. Zhao, K.; Yang, D.; Zeng, P.; Huang, Z.; Wu, W.; Li, B.; Teng, T. Effect of water content on the failure pattern and acoustic emission characteristics of red sandstone. *Int. J. Rock Mech. Min. Sci.* **2021**, *142*, 104709. [CrossRef]
26. Burdine, N. Rock failure under dynamic loading conditions. *Soc. Petrol. Eng. J.* **1963**, *3*, 1–8. [CrossRef]
27. Fuenkajorn, K.; Phueakphum, D. Effects of cyclic loading on mechanical properties of Maha Sarakham salt. *Eng. Geol.* **2010**, *112*, 43–52. [CrossRef]
28. Ma, L.J.; Liu, X.Y.; Wang, M.Y.; Xu, H.F.; Hua, R.P.; Fan, P.X.; Jiang, S.R.; Wang, G.A.; Yi, Q.K. Experimental investigation of the mechanical properties of rock salt under triaxial cyclic loading. *Int. J. Rock Mech. Min. Sci.* **2013**, *62*, 34–41. [CrossRef]
29. Pujades, E.; Willems, T.; Bodeux, S.; Orban, P.; Dassargues, A. Underground pumped storage hydroelectricity using abandoned works (deep mines or open pits) and the impact on groundwater flow. *Hydrogeol. J.* **2016**, *24*, 1531–1546. [CrossRef]
30. Wu, Q.; Liu, Y.; Tang, H.; Kang, J.; Wang, L.; Li, C.; Wang, D.; Liu, Z. Experimental study of the influence of wetting and drying cycles on the strength of intact rock samples from a red stratum in the Three Gorges Reservoir area. *Eng. Geol.* **2023**, *314*, 107013. [CrossRef]
31. Hashash, Y.; Hook, J.; Schmidt, B.; John, I.; Yao, J. Seismic design and analysis of underground structures. *Tunn. Undergr. Space Technol.* **2001**, *16*, 247–293. [CrossRef]
32. Liu, E.; He, S. Effects of cyclic dynamic loading on the mechanical properties of intact rock samples under confining pressure conditions. *Eng. Geol.* **2012**, *125*, 81–91. [CrossRef]
33. Erarslan, N.; Alehossein, H.; Williams, D.J. Tensile fracture strength of Brisbane tuff by static and cyclic loading tests. *Rock Mech. Rock Eng.* **2014**, *47*, 1135–1151. [CrossRef]
34. Eberhardt, E.; Stead, D.; Stimpson, B. Quantifying progressive pre-peak brittle fracture damage in rock during uniaxial compression. *Int. J. Rock Mech. Min. Sci.* **1999**, *36*, 361–380. [CrossRef]
35. Trippetta, F.; Collettini, C.; Meredith, P.; Vinciguerra, S. Tectonophysics evolution of the elastic moduli of seismogenic triassic evaporites subjected to cyclic stressing. *Tectonophysics* **2013**, *592*, 67–79. [CrossRef]
36. Tien, Y.; Lee, D.; Juang, C. Strain, pore pressure and fatigue characteristics of sandstone under various load conditions. *Int. J. Rock Mech. Min. Sci. Geomech. Abstr.* **1990**, *27*, 283–289. [CrossRef]
37. Alkan, H.; Cinar, Y.; Pusch, G. Rock salt dilatancy boundary from combined acoustic emission and triaxial compression tests. *Int. J. Rock Mech. Min. Sci.* **2007**, *44*, 108–119. [CrossRef]
38. Meng, Q.; Zhang, M.; Zhang, Z.; Han, L.; Pu, H. Research on non-linear characteristics of rock energy evolution under uniaxial cyclic loading and unloading conditions. *J. Environ. Geol.* **2019**, *78*, 650.1–650.20. [CrossRef]
39. Tham, L.G.; Liu, H.; Tang, C.A.; Lee, P.K.K.; Tsui, Y. On Tension Failure of 2-D Rock Specimens and Associated Acoustic Emission. *J. Rock Mech. Rock Eng.* **2005**, *38*, 1–19. [CrossRef]
40. Aggelis, D.G. Classification of cracking mode in concrete by acoustic emission parameters. *Mech. Res. Commun.* **2011**, *38*, 153–157. [CrossRef]
41. Nejati, H.R.; Nazerigivi, A.; Sayadi, A.R. Physical and mechanical phenomena associated with rock failure in Brazilian disc specimens. *Int. J. Environ. Chem. Ecol. Geol. Geophys. Eng.* **2018**, *12*, 35–39.

42. Federation of Construction Materials Industries. *JCMS-III B5706 Monitoring Method for Active Cracks in Concrete by Acoustic Emission*; Federation of Construction Materials Industries: Japan, Tokyo, 2003.
43. Ohno, K.; Ohtsu, M. Crack classification in concrete based on acoustic emission. *J. Constr. Build. Mater.* **2010**, *24*, 2339–2346. [CrossRef]
44. Gan, Y.X.; Wu, S.C.; Ren, Y.; Zhang, G. Evaluation indexes of granite splitting failure based on RA and AF of AE parameters. *J. Rock Soil Mech.* **2020**, *41*, 2324–2332. (In Chinese)